Electronic supplementary information

Cobalt Silicate: Critical Synthetic Condition Affect Its Electrochemical Properties for Energy Storage and Conversion

Tao Hu, Yang Wang, Xueying Dong, Yang Mu, Xiaoyu Pei, Xuyang Jing, Miao Cui, Changgong Meng, Yifu Zhang*

State Key Laboratory of Fine Chemicals, School of Chemical Engineering, Dalian University of Technology, Dalian, 116024, China

*E-mail addresses: yfzhang@dlut.edu.cn (Y. Zhang)

Experimental section

Characterizations

The phase was confirmed by Powder X-ray diffraction (XRD) measurements acquired by a Panalytical X'Pert powder diffractometer Ni-filtered Cu Kα radiation (λ = 1.5418 Å, 40 kV, 40 mA) in the 2Theta range from 5° to 80°. The spherical morphology and nano-size were characterized by field emission scanning electron microscope (FE-SEM, NOVA Nano SEM 450, FEI), which Energy-dispersive X-ray spectrometer (EDS) and elemental mapping were recorded by likewise. The samples for SEM were platinum-sputtered. And hollow spherical morphology was confirmed by transmission electron microscopy (TEM, FEITecnai F30, FEI). The samples for TEM were dispersed in a mixture of 5 mL deionized water and 10 mL ethanol. Specific surface area of the products was confirmed by Nitrogen adsorption isotherm measurements which were carried out by Brunauer-Emmet-Teller (BET) method. The samples were heated over night at 100 ℃ for dehydration. Ultraviolet–visible spectroscopy (UV–Vis) were collected on a Hitachi U-3900/3900H scanning spectrophotometer with an integrated sphere. The X-ray photoelectron spectroscopy (XPS) measurements were excited using Al Kα radiation with a passing energy of 20 eV on an ESCALAB 250Xi electron spectrometer.

Fig. S1

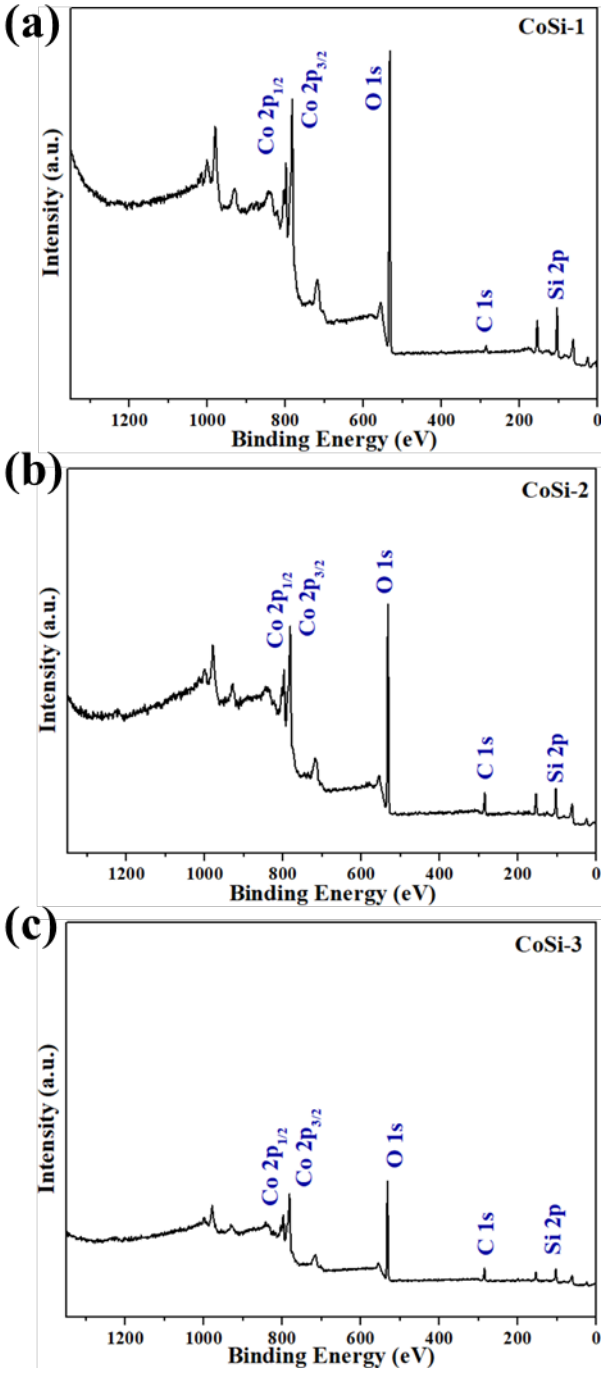

Fig. S1. XPS surveys of CoSi-1 (a), CoSi-2 (b), CoSi-3-3 (c).

Fig. S2

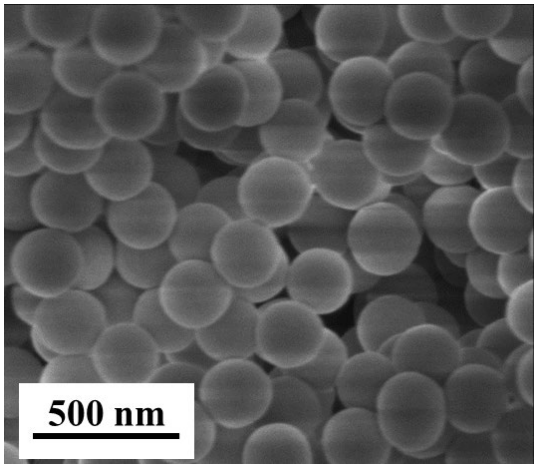

Fig. S2. SEM image of Stöber SiO_2.

Fig. S3

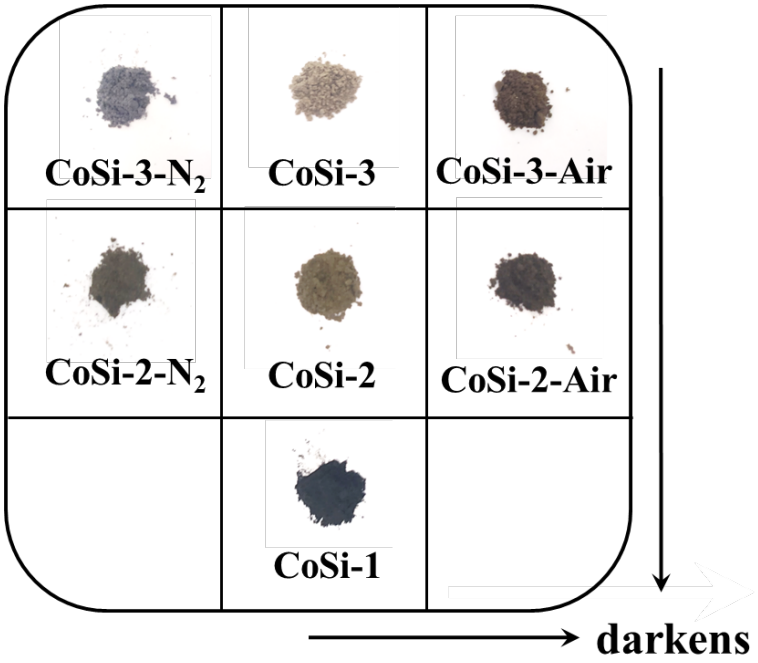

Fig. S3. Colors of CoSi-1, CoSi-2, CoSi-3, CoSi-2-Air, CoSi-2-N_2, CoSi-3-Air and CoSi-2-N_2.

Fig. S4

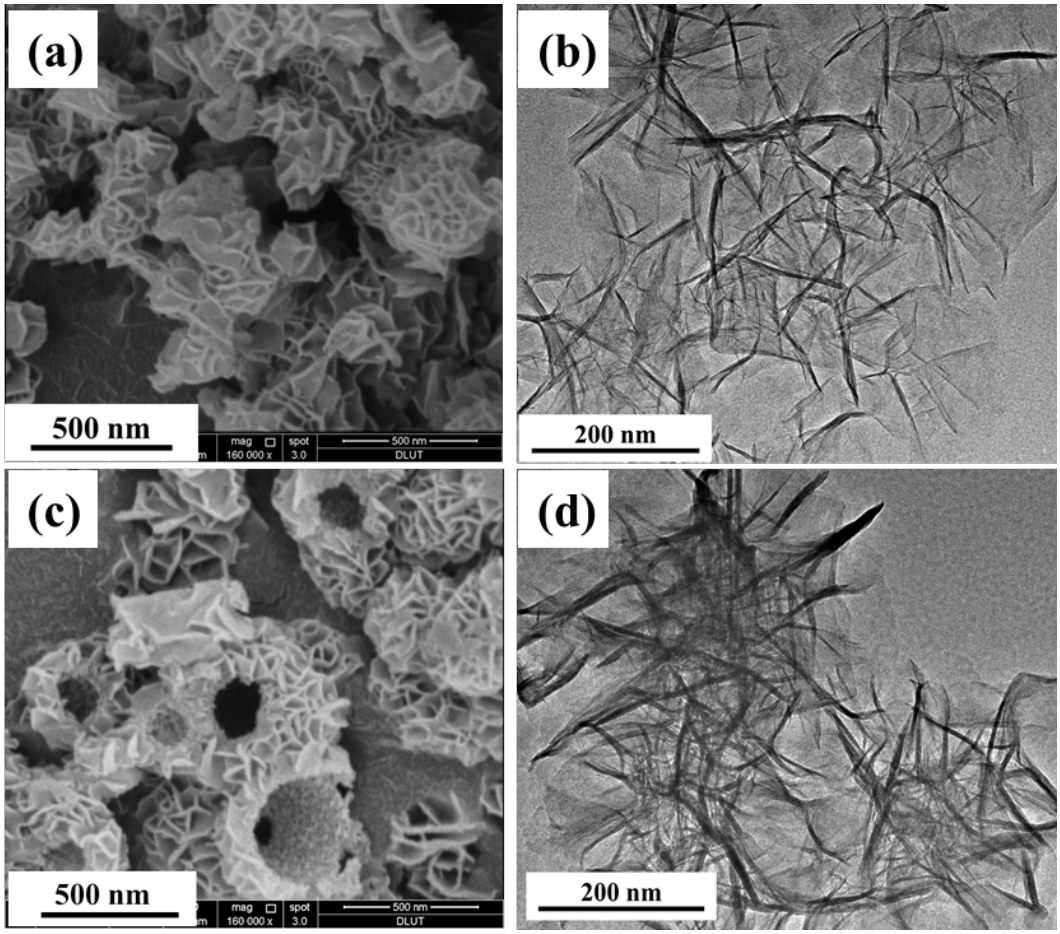

Fig.S4. (a, b) SEM and TEM images of CoSi-3(4h); (c, d) SEM and TEM images of CoSi-3(12h).

Fig. S5

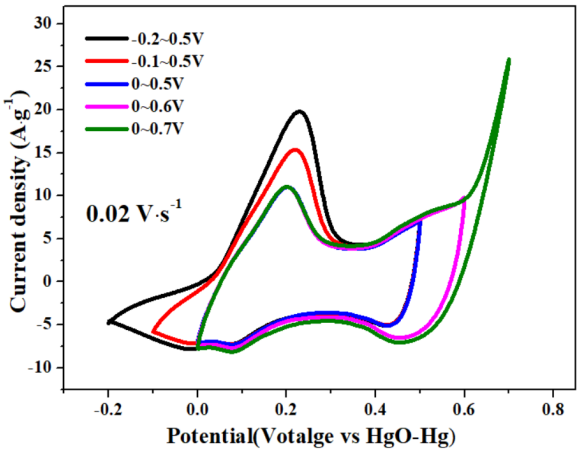

Fig. S5. Selection of potential regions.

Fig. S6

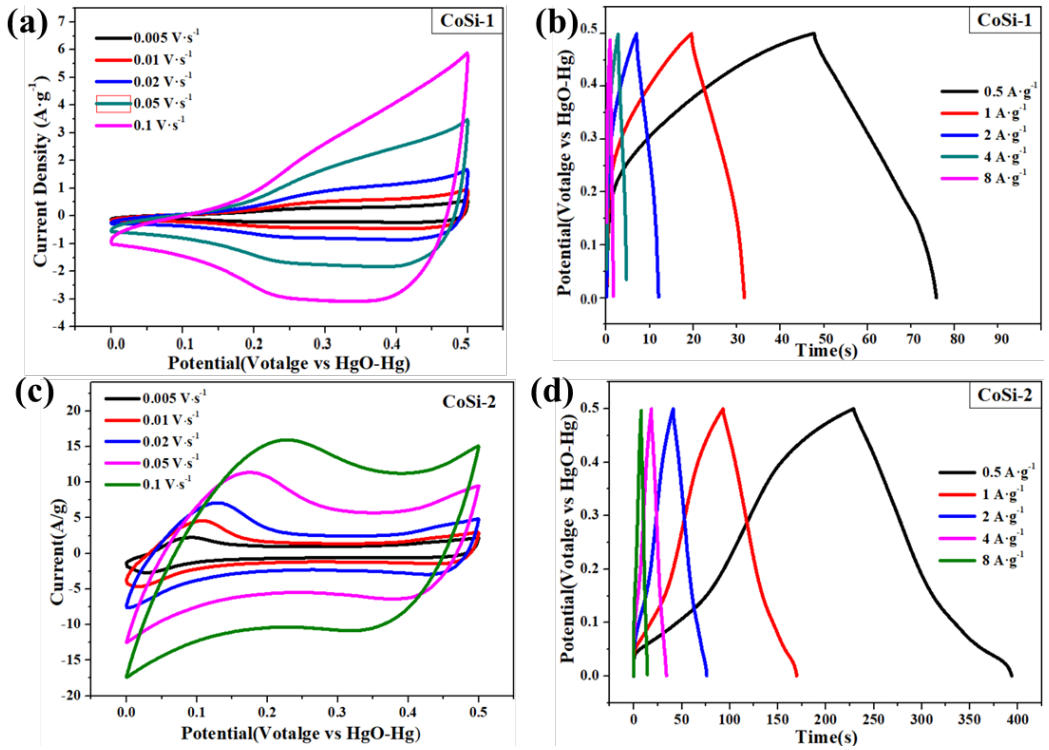

Fig. S6. (a, c) CV curves at different scan rates of CoSi-1 and CoSi-2, (b, d) GCD curves at different current densities of CoSi-1 and CoSi-2.

Fig. S7

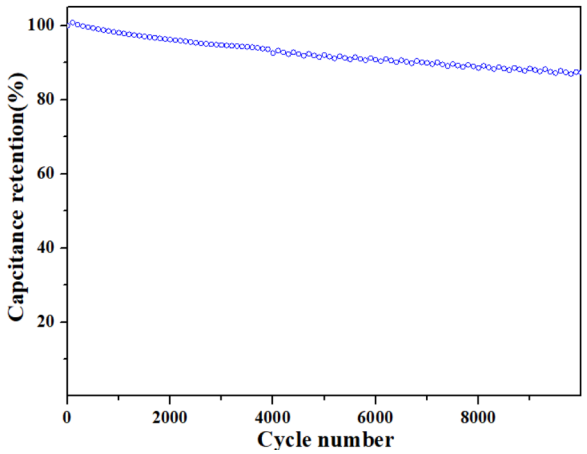

Fig. S7. Cycle performance of CoSi-3.

Fig. S8

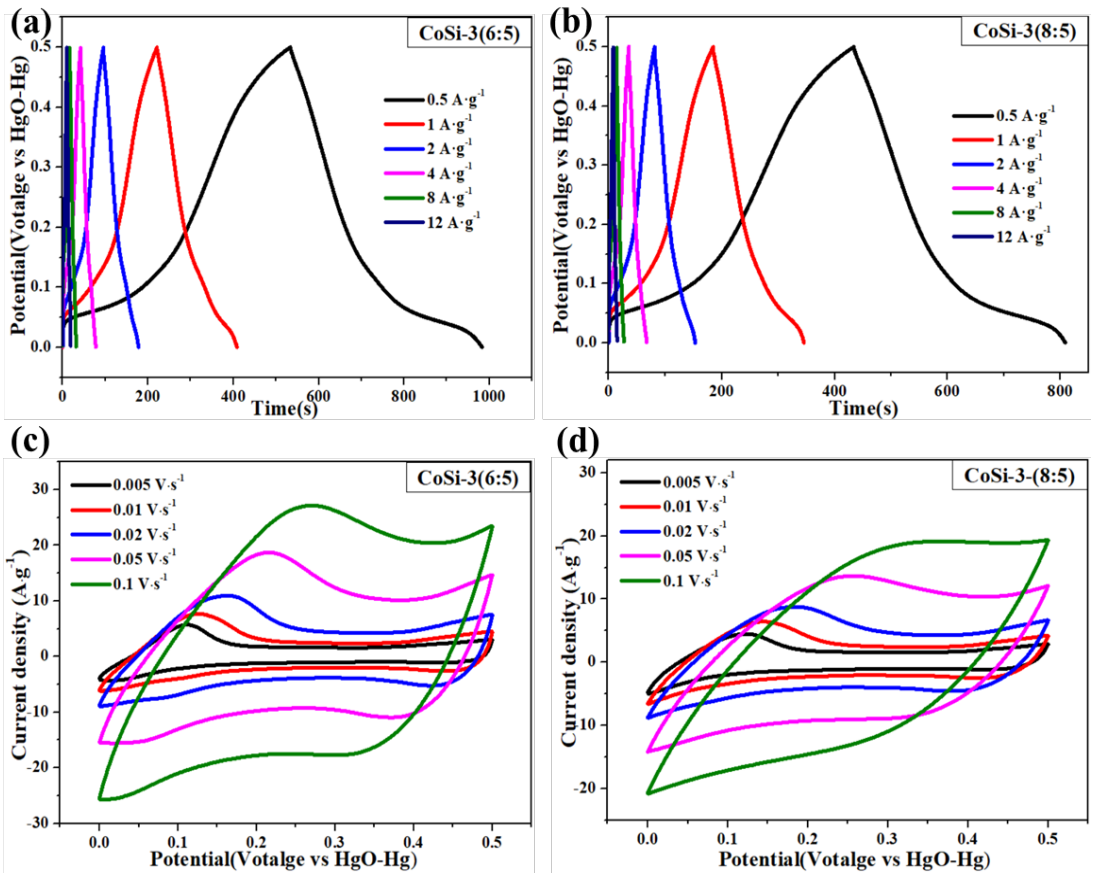

Fig. S8. (a, b) GCD curves at different current densities of CoSi-3(6:5) and CoSi-3(8:5), (c, d) CV curves at different scan rates of CoSi-3(6:5) and CoSi-3(8:5).

CV and GCD curves of CoSi-3(6:5) and CoSi-3(8:5) are shown in Figure S8. CoSi-3(6:5) shows the capacitive performance of 492, 408, 356, 310, 254 and 214 $F \cdot g^{-1}$ at current density of 0.5, 1, 2, 4, 8 and 12 $A \cdot g^{-1}$ (Figure S8a). CoSi-3(8:5) shows the capacitive performance of 404, 346, 306, 269, 215 and 179 $F \cdot g^{-1}$ at current density of 0.5, 1, 2, 4, 8 and 12 $A \cdot g^{-1}$ (Figure S7b). CV curves at 20 $mV \cdot s^{-1}$ and GCD curves at 0.5 $A \cdot g^{-1}$ of CoSi-3, CoSi-3(6:5) and CoSi-3(8:5) are compared in Figure S8. CoSi-3(6:5) shows the largest areas of CV curve and the highest specific capacitance. The variation trend of capacitance is consistent with that of specific surface area, indicating that the capacitance performance is positively correlated with specific surface area.

Fig. S9

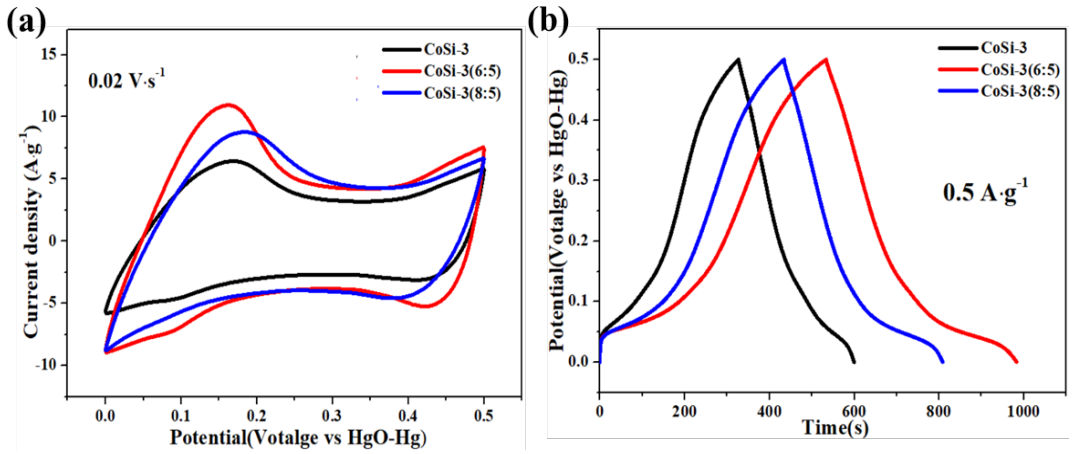

Fig. S9. (a) CV curves at scan rate of 20 mV·s^{-1} of CoSi-3, CoSi-3(6:5) and CoSi-3(8:5), (b) GCD curves at current densities of 0.5 A·g^{-1} of CoSi-3, CoSi-3(6:5) and CoSi-3(8:5).

Table S1

Table 1. Comparison of electrochemical properties of CoSi-3 and cobalt silicates reported in the literatures.

Materials	Electrolyte	Potential range/V	Specific capacitance	Cycle	Ref.
CoSi-3	3 M KOH	0~0.5	301 $F \cdot g^{-1}$ at 0.5 $A \cdot g^{-1}$	86 % after 10000 cycles	This work
$Co_xNi_{3-x}Si_2O_5(OH)_4$/C	3 M KOH	−0.8~0.6	226 $F \cdot g^{-1}$ at 0.5 $A \cdot g^{-1}$	99 % after 10000 cycles	1
bulk Co_2SiO_4	3 M KOH	−0.2~0.8	217 $F \cdot g^{-1}$ at 0.5 $A \cdot g^{-1}$	–	2
Co_2SiO_4 nanobelts	3 M KOH	−0.2~0.8	244 $F \cdot g^{-1}$ at 0.5 $A \cdot g^{-1}$	–	2
$Co_3(Si_2O_5)_2(OH)_2$	6 M KOH	0.1~0.55	237 $F \cdot g^{-1}$ at 5.7 $mA \cdot cm^{-2}$	95 % after 150 cycles	3
$Co_3Si_2O_5(OH)_4$	6 M KOH	0~0.5	570 $F \cdot g^{-1}$ at 0.7 $A \cdot g^{-1}$	–	4
$(Ni, Co)_3Si_2O_5(OH)_4$	1M KOH	0~0.5	144 $F \cdot g^{-1}$ at 1 $A \cdot g^{-1}$	99 % after 10000 cycles	5
Ni-Co silicate hollow sphere	2 M KOH	0.05~0.4	215.92 $F \cdot g^{-1}$ at 1 $A \cdot g^{-1}$	86 % after 5000 cycles	6
Co_2SiO_4@Co_2SiO_4/rGO	3 M KOH	−0.2~0.8	483 $F \cdot g^{-1}$ at 0.5 $A \cdot g^{-1}$	58 % after 10000 cycles	2
Co_2SiO_4@MnO_2	3 M KOH	−0.5~0.6	490.5 $F \cdot g^{-1}$ at 1 $A \cdot g^{-1}$	80 % after 5000 cycles	7
Co_2SiO_4@$MnSiO_3$	3 M KOH	−0.1~0.55	309 $F \cdot g^{-1}$ at 0.5 $A \cdot g^{-1}$	64 % after 10000 cycles	8
Co_2SiO_4/$Ni(OH)_2$	3 M KOH	−0.1~0.55	1101 $F \cdot g^{-1}$ at 1 $A \cdot g^{-1}$	46 % after 4000 cycles	9

References

1 Y. F. Zhang; C. Wang; H. M. Jiang; Q. S. Wang; J. Q. Zheng and C. G. Meng, *Chem. Eng. J.*, **2019**, *375*, 121938.

2 Y. Cheng; Y. F. Zhang; H. M. Jiang; X. Y. Dong; C. G. Meng and Z. K. Kou, *J. Power Sources*, **2020**, *448*, 227407.

3 G. Q. Zhang; Y. Q. Zhao; F. Tao and H. L. Li, *J. Power Sources*, **2006**, *161*, 723-729.

4 J. H. Zhao; Y. J. Zhang; T. Wang; P. W. Li; C. Z. Wei and H. Pang, *Adv. Mater. Interfaces*, **2015**, *2*, 1400377.

5 Q. Rong; L. L. Long; X. Zhang; Y. X. Huang and H. Q. Yu, *Appl. Energy*, **2015**, *153*, 63-69.

6 F. Y. Dong; X. J. Liu and X. Z. Sun, *ChemistrySelect*, **2019**, *4*, 5258-5263.

7 Y. F. Zhao; Y. F. Zhang; Y. Cheng; F. P. Tian; H. M. Jiang; X. Y. Dong and C. G. Meng, *Colloid Surf. A-Physicochem. Eng. Asp.*, **2020**, *600*, 124951.

8 Y. Cheng; Y. F. Zhang; H. M. Jiang; X. Y. Dong; J. Q. Zheng and C. G. Meng, *J. Colloid Interface Sci.*, **2020**, *561*, 762-771.

9 Y. F. Zhao; Y. F. Zhang; Y. Cheng; W. S. Zhao; W. J. Chen; C. G. Meng and C. Huang, *Mater. Lett.*, **2021**, *282*, 128774.